

Contents lists available at ScienceDirect

HardwareX

journal homepage: www.elsevier.com/locate/ohx





An open-hardware community ice nucleation cold stage for research and teaching

Sunandan Mahant ^{a,1}, Shweta Yadav ^b, Cameron Gilbert ^a, Eva R. Kjærgaard ^c, Mads M. Jensen ^c, Tommy Kessler ^c, Merete Bilde ^c, Markus D. Petters ^{a,1,*}

- ^a Department of Marine, Earth, and Atmospheric Sciences, North Carolina State University, Raleigh, NC 27695-8208, USA
- ^b Department of Environmental Sciences, Central University of Jammu, Samba, Jammu, J&K 181143, India
- ^c Department of Chemistry, Aarhus University, Aarhus, Denmark

ARTICLE INFO

Keywords: Ice nucleation Aerosol technology Aerosol science Cold stage Drop freezing assay

ABSTRACT

Aerosol particles with rare specific properties act as nuclei for ice formation. The presence of ice nucleating particles in the atmosphere leads to heterogeneous freezing at warm temperatures and thus these particles play an important role in modulating microphysical properties of clouds. This work presents an ice nucleation cold stage instrument for measuring the concentration of ice nucleating particles in liquids. The cost is \sim \$10 k including an external chiller. Using a lower cost heat sink reduces the cost to \sim \$6 k. The instrument is suitable for studying ambient ice nucleating particle concentrations and laboratory-based process-level studies of ice nucleation. The design plans allow individuals to self-manufacture the cold-stage using 3D printing, off-the-shelf parts, and a handful of standard tools. Software to operate the instrument and analyze the data is also provided. The design is intended to be simple enough that a graduate student can build it as part of a course or thesis project. Costs are kept to a minimum to facilitate use in classroom demonstrations and laboratory classes.

Specifications table

Hardware name	Community Ice Nucleation Cold Stage
Subject area	 Environmental, planetary and agricultural sciences
	 Educational tools and open source alternatives to existing infrastructure
Hardware type	 Measuring physical properties and in-lab sensors
	 Aerosol sampling equipment
Closest commercial analog	Not Available
Open source license	GNU General Public License v3.0
	CERN Open Hardware Licence Version 2 - Strongly Reciprocal
Cost of hardware	\$10,000
	(continued on post page)

(continued on next page)

https://doi.org/10.1016/j.ohx.2023.e00491

 $Received\ 5\ July\ 2023;\ Received\ in\ revised\ form\ 15\ October\ 2023;\ Accepted\ 10\ November\ 2023$

Available online 11 November 2023

2468-0672/© 2023 The Authors. Published by Elsevier Ltd. This is an open access article under the CC BY-NC-ND license (http://creativecommons.org/licenses/by-nc-nd/4.0/).

^{*} Corresponding author.

E-mail address: markus.petters@ucr.edu (M.D. Petters).

¹ Now at: Department of Chemical and Environmental Engineering, University of California Riverside, Riverside, CA 92521, USA.

(continued)

Hardware name	Community Ice Nucleation Cold Stage	
Source file repositories	https://doi.org/10.5281/zenodo.7893503	
	https://doi.org/10.5281/zenodo.7765110	
	https://doi.org/10.5281/zenodo.7765115	
	https://doi.org/10.5281/zenodo.7765097	
	https://doi.org/10.5281/zenodo.8011609	
	https://doi.org/10.5281/zenodo.8011611	

Hardware in context

Atmospheric aerosols play a central role in cloud physics. Specifically, the formation of cloud droplets and ice crystals is strongly tied to the chemical and physical nature of the atmospheric aerosol. The historical development of these ties were recently reviewed by Kreidenweis et al. [1]. Ice nucleation can occur in several distinct modes [2,3], including homogeneous nucleation from a liquid, heterogeneous freezing nucleation on particles immersed in a droplet (immersion freezing), deposition freezing nucleation and contact freezing nucleation. For clouds warmer than -38 °C, ice nucleating particles (INPs) are needed to initiate first ice formation via some heterogeneous freezing nucleation process. There has been a strong interest in studying atmospheric ice nucleation processes, resulting in approximately exponential growth in published ice nucleation research over the last two decades [1].

Although there is a plethora of different INP instrument designs [4], three main measurement principles have emerged. Expansion or mixing cloud chambers [5,6], continuous flow diffusion chambers [7–10], and cold-stage techniques (e.g. [11–17]). Cloud chambers and diffusion chambers are expensive to build, require significant maintenance, and require skilled personnel to operate the instruments. The construction of a continuous flow diffusion chamber, like the Colorado State University (CSU) design [7] requires significant financial resources and technical expertise to build. In contrast, cold-stage techniques are much simpler and less expensive to build. Although the technique has been in use for decades [14], and many new cold-stage setups have been reported in the literature over the past 10 years (see [11,30,44,45] and references therein), commercial versions are not available to the knowledge of the authors.

The cold stage instrument featured here is an offline method for INP measurement that works on the principle of the Drop Freezing Assay Technique [14]. Briefly, a bulk liquid sample is subdivided into droplets. These droplets are placed on a surface, the surface is cooled, and the freezing temperature of the droplet is detected and recorded typically via optical means. The INP concentration in the

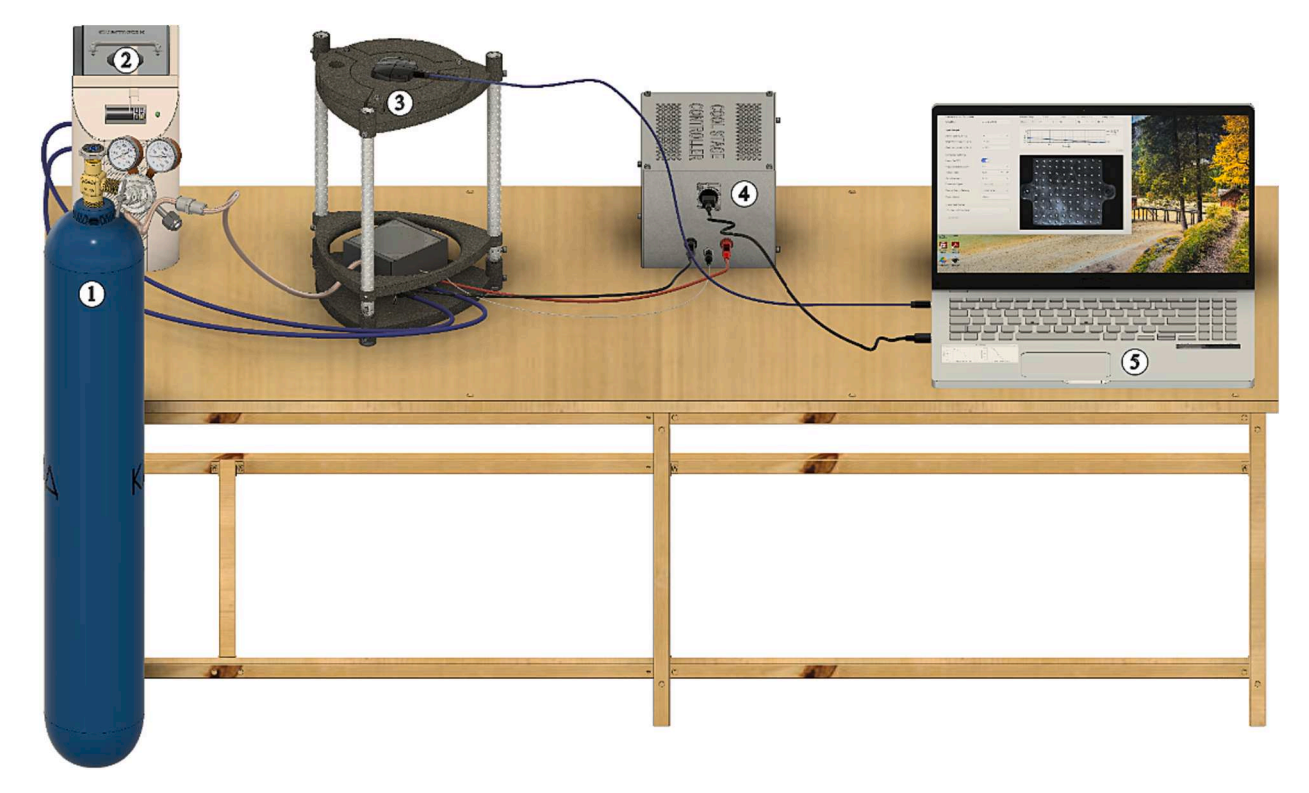


Fig. 1. Schematic of the fully assembled cold stage instrument setup. 1: N₂ cylinder, 2: chilled-bath circulator, 3: cold stage assembly, 4: cold stage controller, 5: data acquisition computer.

liquid is then calculated using the method of Vali [18].

The principle of the cold-stage instrument proposed is suited to study deposition [19–22], immersion [23–25], and contact freezing modes [26–29]. The cold-stage technique has proven to be a highly effective tool to study ice nucleation of atmospheric mimics in the laboratory, to carry out process-level studies probing questions such as nucleation rates, active site densities, stochastic vs. deterministic elements of freezing, contact freezing, and importantly, measuring the concentration of atmospheric INP concentrations [24,30–34]. Since aerosol is collected on filters or with impingers, and filter samples are relatively easily obtained, the technique has been used to measure INP concentration from many popular sampling platforms including ships [35], unmanned aerial vehicles [36], balloons [37], aircrafts [38], and ground-based sites [24,31]. In addition to its utility in the Atmospheric Sciences, the cold-stage technique has perhaps surprising applications in many other fields that need to control nucleation during cooling [39–41].

The context for this work is that almost all ice nucleation instruments, including cold-stages, are custom built and are developed by individual research groups. To our knowledge no cold-stage instruments have been made available commercially. This limits participation in ice nucleation research to groups that specialize in instrument development, or groups that have access to purchase expensive equipment. Here we report a moderately low cost, portable and easy to use cold stage instrument. The design of the instrument is built upon several iterations of the technique [12,23–25,31,32,42,43], which has been validated in several intercomparison studies [11,30,44,45]. Herein, the original designs of the instrument have been adapted to be manufactured using 3D printing and standard off-the-shelf components and pieces. The software stack, including data acquisition software and drivers have been rewritten to include only free and open source software. Combined this significantly lowers the cost of building the instrument.

Hardware description

Fig. 1 shows a schematic of the complete cold stage instrument setup. The main components of the setup include (1) supply of dry N_2 from a cylinder, (2) a chilled-bath circulator used as a heat sink, (3) the cold stage stand assembly used to conduct the experiment, (4) a power supply/control box for temperature control, and (5) a computer for data acquisition and analysis. The cold stage stand holds a camera and the coldstage core cell. Inside the cell is a metal plate that is cooled with a thermoelectric cooler (TEC). The cold stage cell is connected to the power supply/control box. A thermistor reports temperature at the metal surface. The cold stage controller box supplies DC power to control the TEC. The box is connected to the computer via a USB cable for electronic communication. Similarly, the camera is connected to the computer for saving droplet images. The bottom of the TEC is heatsinked using liquid flow from the circulating liquid bath. Finally, the cell is supplied with dry N_2 flow to prevent condensation of water inside the cell during analysis.

The intended use of the setup is to measure the INP concentration in supercooled liquid water. Liquid droplets of known volume are placed on the cold surface. The surface is cooled at a constant rate, typically at 1-2 K min $^{-1}$. Time lapse photography is used to record images of the drops every few seconds. When the droplets freeze, they turn opaque. The change in brightness is detected using an automated image detection code. The instrument is suitable for studying ambient INP concentrations and laboratory-based process-level studies of the nucleation process.

Design files summary

An overview of the repositories for the cold stage stand, cell as well as control and analysis software files are provided in Table 1. Each repository contains multiple files. The repositories listed in Table 1 fall into two broad categories, design files and software. The coldStageDesign repository includes the FreeCAD design files for all 3D printed parts. These can be modified as desired. Stereolithography (STL) files are included to facilitate quick 3D printing.

The software stack is organized as follows. All software is written in the Julia language [46]. The language is free and open source software and distributed under the permissive MIT license. The software was written to be executed on a computer with Linux as the operating system, which is free and open source software. All installation instructions are written for this use case. It is possible to run the software on Windows computers, but this specific use case is minimally documented in order to maintain coherency and simplicity in the already complex install instructions.

A package in the Julia language is a bundle of modules and documentation that extends the language functionality. Here, device drivers are shared as Julia packages. The two device shared drivers handle low level communication with the temperature controller (TE Technology TC-36-25-RS232) and the camera (IDS Imaging IDS-U3-3680XLE-C-HQ). These are named *TETechTC3625RS232.jl* and

Table 1 Summary of design repositories.

Design file name	File type	Open source license	Location of the file
coldStageDesign	CAD and STL files	CERN-OHL-S-2.0 ^a	https://doi.org/10.5281/zenodo.7893503
TETechTC3625RS232.jl	Source code	GPLv3 ^b	https://doi.org/10.5281/zenodo.7765110
IDSpeak	Source code	GPLv3 ^b	https://doi.org/10.5281/zenodo.7765115
DropFreezingDetection.jl	Source code	GPLv3 ^b	https://doi.org/10.5281/zenodo.7765097
csDAQ	Source code	GPLv3 ^b	https://doi.org/10.5281/zenodo.8011609
deploy-cif	Container file	GPLv3 ^b	https://doi.org/10.5281/zenodo.8011611

 $^{^{(}a)}$ CERN Open Hardware Licence Version 2 - Strongly Reciprocal.

⁽b)GNU General Public License v3.0.

IDSpeak, respectively.

The csDAQ repository contains the software to control the instrument during regular experimentation. The program uses TETechTC3625RS232.jl and IDSpeak in addition to other external packages that are available as free and open source from standard package repositories. The DropFreezingDetection.jl repository contains software written in the Julia language to analyze images to infer ice nuclei concentration as a function of temperature from ice nucleation cold-stage measurements. This software also depends on other external packages that are available as free and open source from standard package repositories.

Some of these components can be used independently. For example, the *TETechTC3625RS232.jl* can be installed to just communicate with the controller. Installation and use instructions for that package are included with the repository README.md file. Similarly, the *DropFreezingDetection.jl* software can be installed on any computer to perform post processing.

Installing the software stack so that it operates in concert is more involved. For example, the low-level drivers that interface between the *IDSpeak* package and the hardware require the use of a Debian-based distribution or installation from source. This implies that the camera will only function in the *csDAQ* software if the device is appropriately configured and has the required drivers. Synchronization and functioning of all the softwares and drivers simultaneously can be challenging and time consuming even in a Debian-based distribution due to missing/outdated packages or system updates. For this reason, the recommended installation procedure is to use the installation procedure described in the README.md file of the *deploy-cif* repository. Briefly, the procedure requires a computer with a USB v3 port and with a Linux operating system. Installation has been tested on Centos Stream v9, Fedora Linux 38, Ubuntu 23.04, and RedHat Enterprise Linux v9. We expect that the installation procedure will work on most modern Linux distributions. The user will need administrator privileges to complete installation. The first step in the installation is to build a container image. The container image bundles the low-level drivers for the camera and clones the latest version of *csDAQ* and *Drop-FreezingDetection.jl*. Postinstall scripts ensure that all dependencies are downloaded and properly linked. Users that wish to install the entire software stack without the container solution are recommended to use Ubuntu as their Linux distribution and follow the steps in the *Containerfile* and *README.md* files in the *deploy-cif* repository.

Bill of materials summary

Tables 2 and 3 provide information and documentation for costs of the parts needed to construct the cold stage.

Build instructions

Figs. 2, 3, and 4 schematically summarize how to build the instrument. A step by step assembly instruction with pictures is provided in the supporting document. Figs. S1, S2 and S3 in the supplement document are for cold stage cell, cold stage stand, and cold stage controller box respectively. Videos that animate the order of operation are provided in the supporting information. Animation S1 shows a time lapse of the 3D print of the base block. Animation S2 shows the assembly order for Fig. 2. Animation S3 shows the assembly order of Fig. 3. Animation S4 shows the assembly order of Fig. 4.

Cold stage cell

Fig. 2 shows the components and assembly diagram of the cold stage cell. Component details are given in Table 2. The base block (4) is 3D printed (see also Animation S1). There are two narrow openings on the base block to feed thermistors into the cell. One thermistor is fed into the metal block and is used to measure the temperature of the surface. The second thermistor is optional and can be used to monitor temperature anywhere inside the cell. One example use of a second thermistor is to measure the temperature of an oil/water suspension that is placed in a crucible sitting on the metal surface [12]. In this application, the purpose is to quantify the thermal lag between the primary thermistor and the temperature of the suspension. Dry N_2 is used to prevent condensation inside the

Table 2Bill of materials for the cold stage cell. Reference number after each component, e.g. (1) corresponds to the number label in Fig. 2. Prices are in USD.

Designator	Component	Quantity	Cost per unit	Total cost	Source	Material type
WBA-1.62-0.55-CU-01	Heat sink (1)	1	\$102.50	\$102.50	(a)	Copper
WBF-1.16-3.16-NY	Barbed Tube Fitting (2)	2	\$5.00	\$10.00	(a)	Nylon
25412-5L31-07CQQ	TEC Element (3)	1	\$76.00	\$76.00	(a)	N/A
Body.stl	Base Block (4)	1	\$5.00	\$5.00	(b)	Plastic
CPT-2.25-1.62-0.25-AL	Cold Plate 5	1	\$27.75	\$27.75	(a)	Aluminum
Spacer.stl	Spacer (6)	2	N/A	\$5.00	(b)	Plastic
$M2.5 \times 25 \text{ mm}$	Screw (7)	2	N/A	\$10.00	(d)	SS
$M4 \times 14 \ mm$	Screw (8)	4	N/A	\$10.00	(d)	SS
#11-855	Glass Cover (9)	1	\$45.50	\$45.50	(c)	Glass
TG-CMQ2-2.7G	Thermal Paste	1	6.50	\$6.50	(a)	Ceramique 2
Total				\$298		

- (a) Custom Thermoelectric: https://customthermoelectric.com/.
- (b) 3D printed, cost estimate is for raw material only.
- (c) Edmund Optics: https://www.edmundoptics.com/.
- (d) Hardware store, packaged in large quantities. SS = Stainless steel.

Table 3 Bill of materials for the cold stage stand. Reference number for each component, e.g. (1) corresponds to the number label in Fig. 3. Prices are in USD.

Designator	Component	Quantity	Cost per unit	Total cost	Source	Material type
Stand_Part1.stl	Base Plate 1	1	N/A	\$5	(a)	PETG
Stand_Part1_s1.stl	Leg for Base Plate 2	3	N/A	\$5	(a)	PETG
Stand_Part1_s2.stl	Plug for Leg (3)	3	N/A	\$5	(a)	PETG
B09NSF5WD7	Tube (15 mm OD \times 12 mm ID, 300 mm L) (4)	3		\$12.69	(b)	Aluminum
Stand_Part2.stl	Stabilizer (5)	1	N/A	\$5	(a)	PETG
Stand_Part3_1.stl	Top Blade 1 (6)	1	N/A	\$5	(a)	PETG
Stand_Part3_2.st	Top Blade 2 (7)	1	N/A	\$5	(a)	PETG
$M4\times25\ mm$	Screw (8)	12	N/A	\$10	(c)	SS
$M5\times35\ mm$	Screw (9)	2	N/A	\$10	(c)	SS
IDS-U3-3680XLE-C-HQ	Camera (10)	1	\$280	\$280	(d)	Electronics
M3 x 25 mm	Screw (11)	2	N/A	\$5	(c)	SS
B08YYGRCBG	M4 Thread Insert (12)	4	N/A	\$18	(b)	Brass
CB-ALY-U3C-SL-03M	USB cable (Gen 3)	1	\$66	\$66	(d)	Electronics
#33-305	Lens	1	\$225	\$225	(e)	Lens
B01531I8IG	Lens adapter	1	\$7.81	\$7.81	(b)	Aluminum
B08YYGRCBG	M4 Thread Insert	4	N/A	\$17.95	(b)	Brass
Total				\$680		

(a) 3D printed, cost estimate is for raw material only: doi: (recommended printing material is Polyethylene terephthalate glycol (PETG) plastic for mechanical strength).

- (b) Amazon: https://www.amazon.com.
- (c) Hardware store, packaged in large quantities. SS = Stainless steel.
- (d) IDS Imaging: https://en.ids-imaging.com/ (2592 x 1944 pixel, 48.0 fps, CMOS color sensor).

 (e) Edmond Optics: https://www.edmundoptics.com/ (UC Series Fixed Focal Length Lens, C-mount, 25 mm focal length, 20 mm working distance).

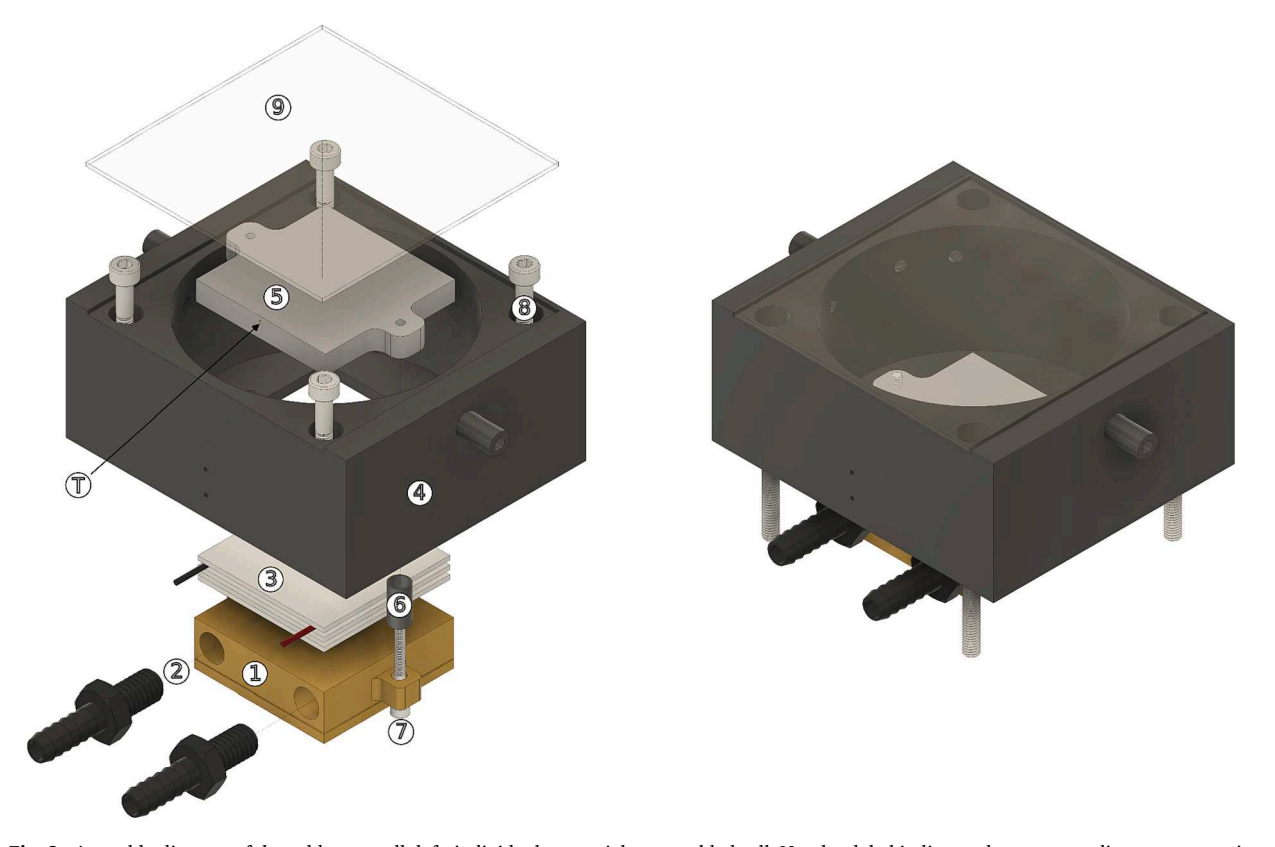


Fig. 2. Assembly diagram of the cold stage cell, left: individual parts, right: assembled cell. Number label indicates the corresponding component in Table 2. 1: heat sink, 2: barb connectors, 3: TEC module, 4: base block, 5: cold plate, 6: spacers, 7: M2.5 screw, 8: M4 screw, 9: glass lid, T: thermistor opening. Two thermistor openings are located on the left front facing side of the baseblock.

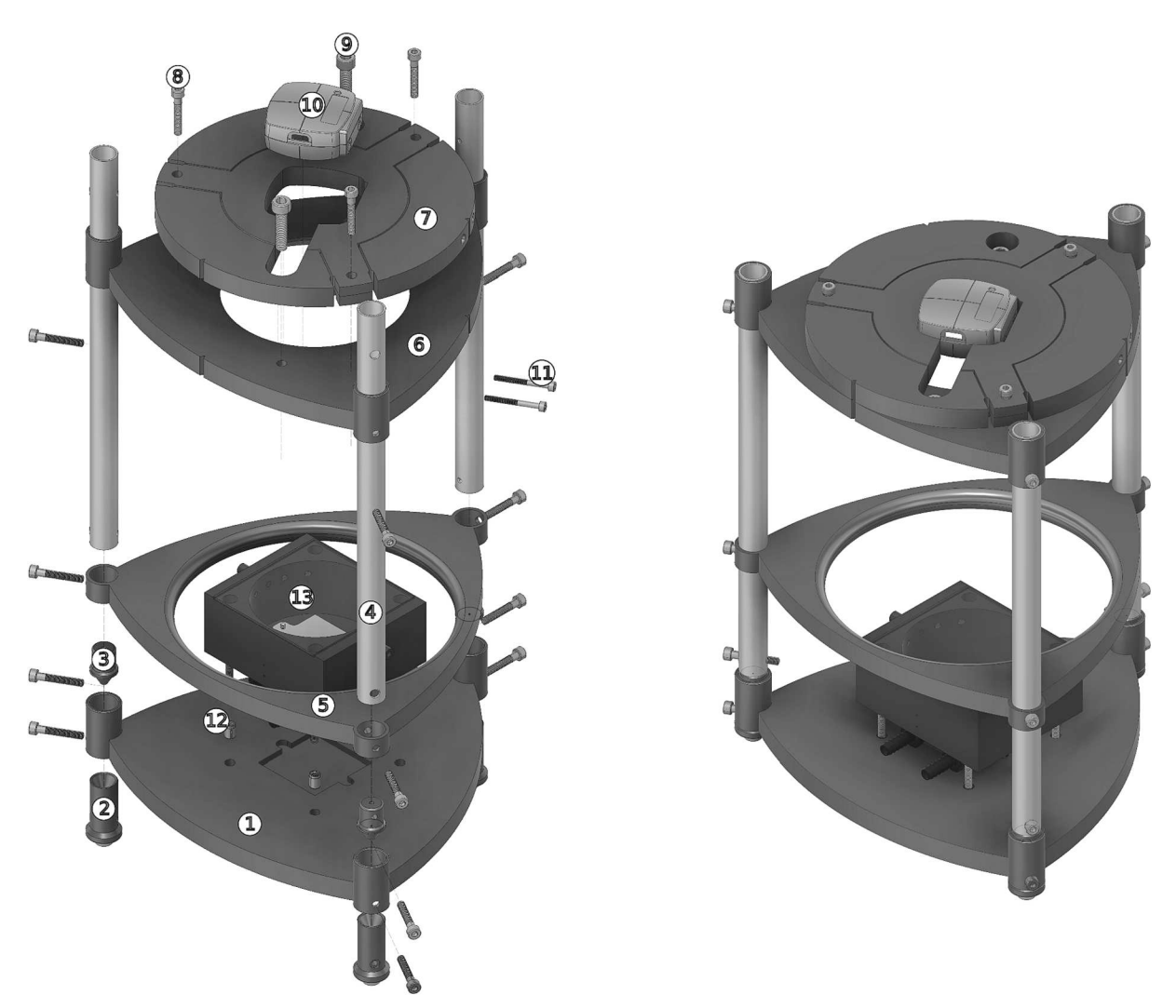


Fig. 3. Assembly diagram of stand for the cold stage stand and cell (in Fig. 2), left: individual parts, right: assembled cell. Number label indicates the corresponding component in Table 3. 1: base plate, 2: leg for base plate, 3: plug for leg, 4: aluminum tube, 5: stabilizer, 6: top plate_1, 7: top plate_2, 8: M4 screw, 9: M5 screw, 10: camera, 11: M3 screw, 12: M4 thread insert, 13: cold stage cell.

cell. The N_2 dry flow is fed into the cell through one of the two protruding ports on parallel sides of the base block, and it vents out through the other port and side leaks. The center body of a cold stage cell consists of three components, the cold metal surface (5), a 2-stage TEC element (3), and a heat sink (1). All three components are placed in a way that the opening for barbed tube fitting in the heat sink, connections of TEC module and thermistor opening in cold metal surface fall on the back side. A removable glass cover (9) prevents ambient air from entering the base block. The glass cover does not seal the cold stage cell perfectly and N_2 can potentially leak from the top.

To assemble the cold stage cell, the TEC element is placed on the heat sink and thermal paste is applied at the interface to ensure optimal heat transfer. Two M2.5 screws (7) are passed through the water block and spacers (6) for obtaining a tight fitting between the heat sink, TEC element and the cold plate. The cold plate is then installed inside the base block. Thermal paste is applied on the TEC module - cold plate interface before installation. Thermistor opening on the printed cell and cold plate should be on the same side. The heat sink is connected to the circulating cooling bath using the barbed tube fitting (2). Four M4 screws (8) are used to secure the cold stage cell to the stand shown in Fig. 3.

Cold stage stand

Fig. 3 shows components and the assembly diagram for the cold stage stand. Component details are given in Table 3. All the components except for the aluminum tubes (5), screws and inserts (8, 9, 11, 12) and camera (10) are 3D printed. The cold stage stand houses the cold stage cell (13) shown in Fig. 2, and helps capture stable pictures of droplets placed on the cold plate inside the cold stage cell. The aluminum rod is mounted to the top plate and the stabilizer, and not the base plate. This makes it easy to quickly isolate

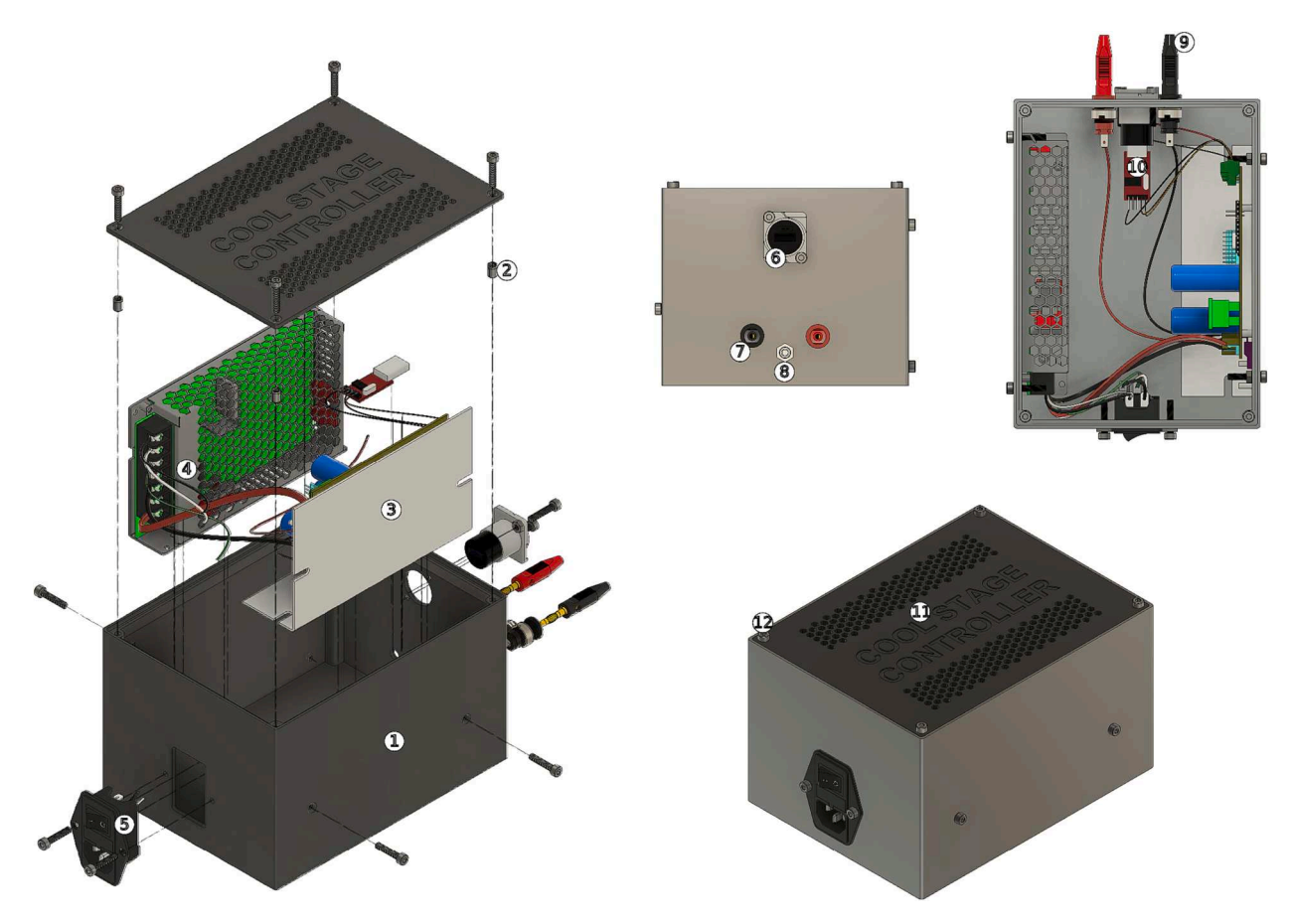


Fig. 4. Assembly diagram of cold stage controller box. Numbered parts and their sources are listed in Table 4. 1: Cold stage controller box, 2: M4 thread insert, 3: temperature controller, 4: DC power supply, 5: rocker switch, 6: USB connector, 7: 4 mm banana socket, 8: 3.5 mm audio mount socket, 9: 4 mm banana plug, 10: USB to RS232, 11: box lid, 12: M4 screw.

Table 4
Bill of materials for the power supply/temperature controller. Reference number for each component, e.g. (1) corresponds to the number in Fig. 4.
Prices are in USD.

Designator	Component	Quantity	Cost per unit	Total cost	Source	Material type
Box_1.stl	Box (1)	1	\$5	\$5	(a)	PETG
B08YYGRCBG	M4 Thread Insert (2)	4	N/A	\$18	(b)	Brass
TC-36-25-RS23	Temperature controller (3)	1	\$615	\$615	(c)	Electronics
LCS150US12	DC Power supply (4)	1	\$26	\$26	(d)	Electrical
B00NWO68JI	Rocker Switch (5)	1	\$8	\$8	(b)	Plastic
B092W8P46Z	USB Pass Through Connector (6)	1	\$14	\$14	(b)	Electronic
B07C7KBZ3S	4 mm Banana Jack Socket (7)	1	N/A	\$12	(b)	Electrical
B07JNC4P7Y	3.5 mm Audio Mount (8)	1	N/A	\$9	(b)	Electrical
B07GL5BVNH	4 mm Banana Plugs (9)	1	N/A	\$12	(b)	Electrical
768-1077-ND	USB to RS232 (10)	1	\$29	\$29	(e)	Electronics
Box_2.stl	Box cover lid (11)	1	\$5	\$5	(a)	PETG
$M4\times15\;mm$	Screw (12)	12	N/A	\$10	(f)	SS
MP-3176	Thermistor	1	\$25	\$25	(c)	Electronics
B01KRO8D20	USB 3.0 Cable, Type A to Type A	1	\$7	\$7	(b)	Electronic
Total	**			\$795		

⁽a) 3D printed, cost estimate is for raw material only: doi: (recommended printing material is Polyethylene terephthalate glycol (PETG) plastic for mechanical strength).

⁽b) Amazon: https://www.amazon.com.
(c) TE Technology: https://tetech.com/.

⁽d) Mouser Electronics: https://www.mouser.com/ (150 W, 12 V, 12.5A DC current).

⁽e) Digikey: $\underline{\text{https://www.digikey.com/}} \text{ (USB-RS232 converter with FTDI chip for Linux compatibility)}.$

 $⁽f) \ Hardware \ store, \ packaged \ in \ large \ quantities. \ SS = Stainless \ steel.$

the base plate so that sample droplets can be placed on the cold plate.

To assemble the cold stage stand, the first step is to install the M4 threaded inserts (12) on the four holes on the base plate 1. This is done by heating up the holes using a soldering station and then quickly installing the metal inserts while the plastic is waxy. Legs for base plate 2 are mounted to the base plate using M4 screws (8). The cold stage cell (13) can then be mounted on the base plate using threaded inserts. Three through holes need to be drilled on each aluminum rod (4). The bottom through hole is to secure the plug for leg (3), the middle is to secure the stabilizer (5) while the top through hole is to secure the top plate_1 (6) using M4 screws (8). The camera assembly is attached to the top plate_2 (7) using two M3 screws (11). The two top plates are attached to each other using two M5 screws (9). Three M4 screws on top plate_2 (7) helps to adjust the positioning of the camera so as to get a good image of the cold plate.

Cold stage controller

Fig. 4 shows the components and assembly diagram of the cold stage controller box and the details of bills of materials used are given in Table 4. The cold stage controller box (1) and its lid (11) are 3D printed. The cold stage box houses the temperature controller (3) and power supply (4). The temperature controller is used to control the temperature of the TEC module and measure temperature of the cold plate in Fig. 2. The temperature controller communicates with the data acquisition computer via a USB connector (6), which in turn converts the signal to RS232 (10). Banana plugs (9) connect power cables of the TEC module to the temperature controller. The thermistors are connected to the controller via an audio socket (8). Table 5 lists component details for items 1, 2 and 5 in Fig. 1 and other miscellaneous items used to complete the setup.

The circuit diagram for all the connections within the cold stage controller box and with the cold stage cell is shown in Fig. 5. The following steps are used to wire it. Rocker Switch 3 Pin IEC320 has 3 wires [green (ground), gray (Neutral) and lime (live)]. The power supply has labels L (live), N (Neutral) and (ground). Step 1 is to screw tight the 3 wires of the rocker switch to respective labeled slots on the power supply. Step 2: The temperature controller has ports WP1, WP2, WP3 and WP4. Ports WP1 and WP2 connect to the TEC module, and WP3 and WP4 connect to the power supply. To supply power from the power supply to the temperature controller, V^+ and V^- from the power supply are connected to the WP3 and WP4 ports of the temperature controller. The temperature controller sends power to the TEC module by connecting V^+ and V^- of the TEC module to WP1 and WP2 ports of the temperature controller. Step 3: Black (V^-) and red (V^+) banana jack sockets are screwed tight through the two corresponding holes in the front panel of the cold stage controller box. The black and red sockets are connected to the black and red banana plugs of the TEC module in the cold stage cell. Step 4: The audio mount socket is screwed to the third hole (below black and red banana sockets) of the cold stage controller box. It is used to connect the thermistor to the temperature controller using a 3.5 mm TRS male plug. Two thermistors can be connected to the temperature controller on ports JP2 using sub ports 1,2 and 5,6. Step 5: A USB3.0 D series panel-mount connector is mounted (above black and red banana sockets) to the cold stage controller box, which is connected to the temperature controller through USB to RS232 cable inside the box.

Table 5
Bill of materials for the setting up and operating of the cold stage as shown in Fig. 1. Reference number for each component, e.g. (1) corresponds to the number in Fig. 1. Prices are in USD.

Designator	Component	Quantity	Cost per unit	Total cost	Source	Material type
Eppendorf Xplorer	Electronic Pipette (0.5–10 μL)	1	\$1000	\$1000	(a)	N/A
22491709	Micropipette tips	1	N/A	\$120	(b)	Plastic
SD07R-20-A11B	Chilled bath circulator (2)	1	\$4400	\$4400	(c)	N/A
	N ₂ Gas Regulator (1)	1	\$250	\$250	(d)	N/A
	Laptop computer (5)	1	\$1000	\$1000	(e)	N/A
B00ANZRT4M	Soldering station	1	\$120	\$120	(f)	N/A
i3 MK3S+	3D Printer	1	\$1100	\$1100	(g)	N/A
IC-4006-13-SS	Critical Orifice	1	\$70	\$70	(h)	Stainless
SS-401-PC	Port connector	2	\$8	\$16	(i)	Stainless
NY-400-SET	Ferrule set	10	N/A	\$17	(i)	Nylon
Total				\$8,100		•

- (a) Eppendorf: https://online-shop.eppendorf.us/ (Manual pipettes are cheaper and sufficient for occasional use).
- (b) Pipette.com: https://pipette.com/.
- (c) Polyscience: https://www.polyscience.com/ (200 W cooling power).
- (d) Regulator Supply: https://regulatorsupply.com/ (CGA 580).
- (e) Dell: https://www.dell.com/ (11th Gen intel i5 CPU or greater, 16 GB RAM, SSD disk).
- (f) Amazon: www.amazon.com (Hakko FX888D-23BY Digital Soldering Station).
- (g) Prusa: https://www.prusa3d.com/.
- (h) O'Keefe Controls Co.: https://www.okeefecontrols.com/.
- (i) Swagelok: https://products.swagelok.com/en/.

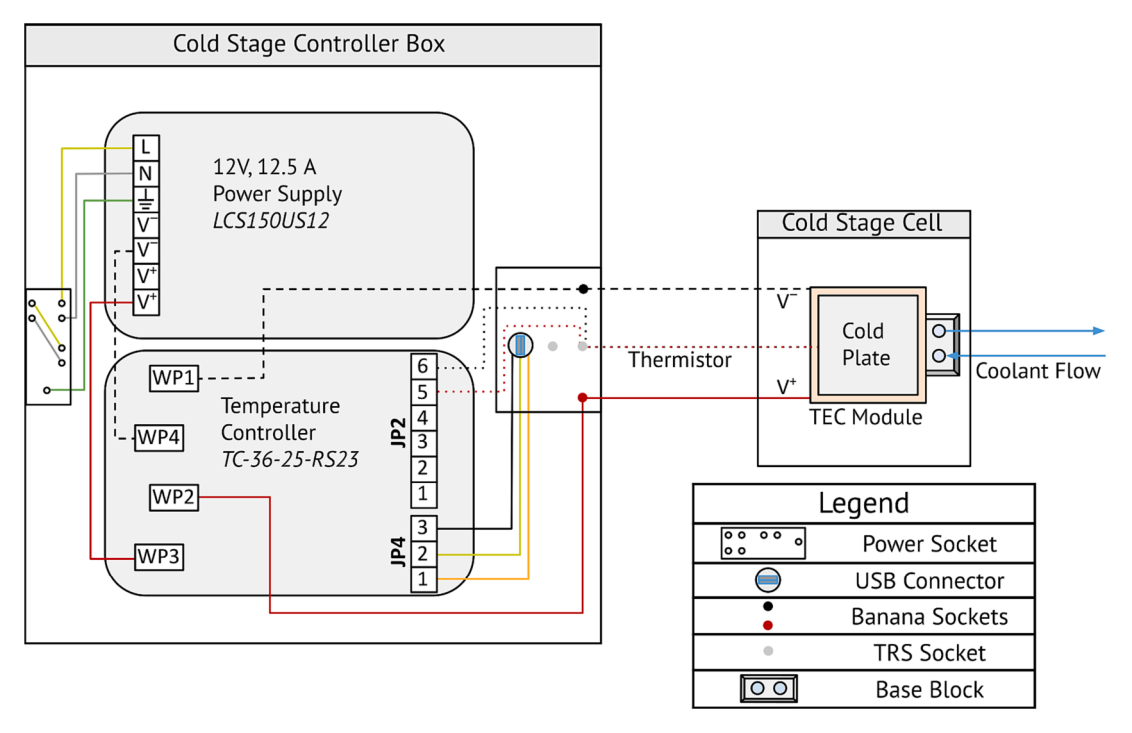


Fig. 5. Circuit diagram of the cold stage controller box and cold stage cell.

Software

Data acquisition and control system

The GUI software written in Julia to control the ice nucleation cold-stage measurements is called *csDAQ*. Using a terminal emulator, navigate to the directory csDAQ/src and start julia with the project flag. To run the program from the shell, run the following command:

[user@host src]\$ julia -project main.jl.

Data processing software

The GUI software written in Julia to analyze drop freezing spectra from ice nucleation cold-stage measurements is called *Drop-FreezingDetection.jl*. Using a terminal emulator, navigate to the directory DropFreezingDetection/src and start julia with the project flag. To run the program from the shell, run the following command:

[user@host src]\$ julia -project main.jl.

Operation instructions

Instrument operation

Before conducting an experiment, ensure that the controller box is powered off at the power switch, and that all wires are connected appropriately. Next turn on the chilled bath circulator and make sure that liquid (water or ethylene glycol) is flowing through the heatsink. This is critical, because powering on the thermoelectric element without cooling will damage the instrument. A thermal cutoff switch (currently not installed) can be inserted to physically cut the power and prevent overheating. Set the temperature of the liquid below 5 °C and check if the thermistor is properly inserted into the hole in the metal plate (thermal paste on the head of the thermistor ensures better contact and heat transfer at the interface).

Nitrogen gas from a cylinder or dry air is needed to prevent condensation. We recommend a flow of $3 \, L \, min^{-1}$ of N_2 from a cylinder, with flow being controlled by a critical orifice. For example, an orifice of 0.013'' (O'Keefe) operated at an upstream pressure of 29 psi (200 kPa) gives a flow of $3 \, L \, min^{-1}$. Low flow of N_2 obviates the need of a pressure relief valve or an oxygen sensor.

Once the drying flow is supplied, start up the data acquisition and control software. Fig. 5 shows an image of the software running during an experiment. After the software has started, make sure that the "Power On/Off" is in the Off position and turn on the controller. Check that the "Read Temperature 1" is reading. Note that "Read Temperature 2" is for logging an optional second thermistor. If no thermistor is supplied, it will read the value corresponding to zero resistance for the specified thermistor type.

Next switch the "Power On/Off" to the On position. This will allow current to flow through the TEC element. The "Read temperature 1" corresponds to the one inserted into the metal block and should quickly approach the "Set Temperature" value. The "Set

Temperature" can be changed to the user's preference. We recommend using $10\,^{\circ}$ C to place the droplets. This minimizes evaporation during the placement of the drops. The value may, however, be too cold to prevent condensation in environments where the dew point temperature exceeds $10\,^{\circ}$ C. Colder temperatures may be used in drier environments.

To perform an experiment, place four siliconized glass square cover slides out of the box [22 mm; HR3-215] on the metal plate. The glass slides provide a hydrophobic surface for sample analysis and are discarded after each experiment. The INP measurements are conducted by placing sample drops on the glass slides. This can be achieved using either an electronic or manual pipette. An electronic pipette is preferred to prevent repetitive strain injury and to increase precision of the drop volume. For a typical experiment, arrays of 5×5 drops each with a volume V = 1 μ L are placed on each slide.

After placing the drops on the slide, close the chamber with the glass lid and place the camera stand above the drop array. The software provides a live feed of the image. Adjust the manual focus of the lens as needed. The image and drop appearance can be adjusted by changing the light intensity, the lens aperture, the camera gain, or the image exposure time. Camera gain and image exposure are currently controlled using text commands. Future versions will expose this feature in the graphical user interface. Once the desired image is achieved, a cooling ramp is started.

The ramp is started by toggling the Manual/Ramp dropdown button. Prior to toggling to the ramp, the user can enter an "Experiment Name" that will be included in the directory name where the saved images are stored. The ramp consists of a linear seasaw ramp between "Start"-"Stop"-"Start", where the "Start" field contains the temperature at the beginning of the ramp and the "Stop" field the lower limit of the ramp. The duration of the scan is specified in the "Duration" field. The "Start" temperature should match the "Set Temperature". Note that the "Duration" is in minutes and corresponds to the full cycle "Start"-"Stop"-"Start". The setting in Fig. 6 corresponds to a ramp from $10~{\rm ^{\circ}C}$ to $-40~{\rm ^{\circ}C}$ to $10~{\rm ^{\circ}C}$ over 50 min. Thus the cooling rate is $2~{\rm ^{\circ}C}$ /min. Once the system is toggled to "Ramp" images are recorded to disk every $2~{\rm s}$. A folder named EXPERIMENT_DATETIME is created for each Ramp in the "Data" directory. Here EXPERIMENT corresponds to the entry in the text field "Experiment Name" and DATETIME is the time stamp of the start of the ramp. The graph can be used to verify that the read temperature closely follows the set temperature during the ramp.

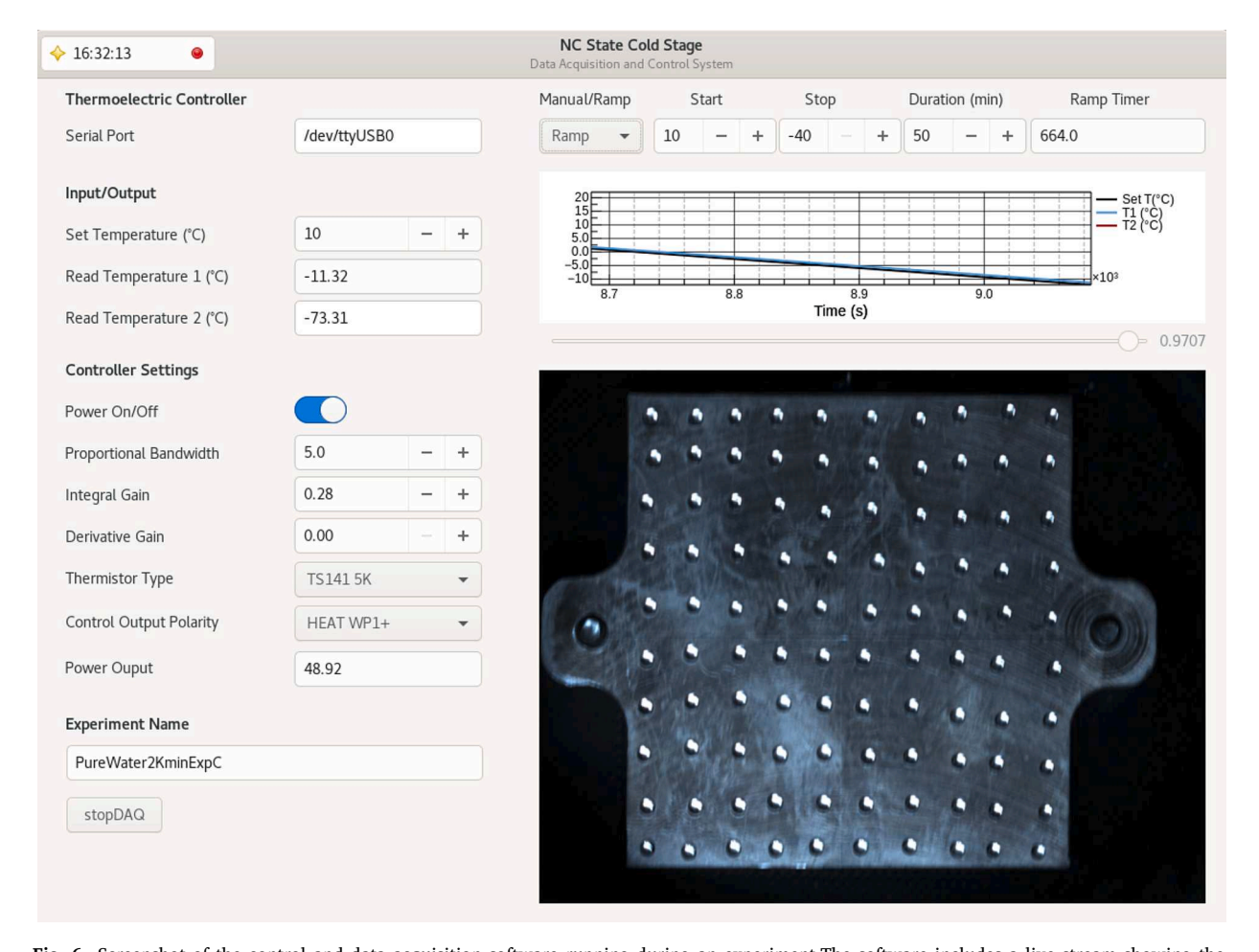


Fig. 6. Screenshot of the control and data acquisition software running during an experiment. The software includes a live stream showing the unfrozen drops placed on hydrophobic slides sitting on the metal surface of the cold plate.

Temperature controller setting

Some, but not all settings of the temperature controller are exposed through the graphical user interface. These include the **Proportional Bandwidth**, the Integral Gain, and the **Derivative Gain** (PID) parameters for the control loop. Those parameters should not require further tuning, but can be adapted for other applications as needed. The thermistor can be exchanged selecting any of the types supported by the hardware, which includes most of the commonly used resistance ranges. The direction of the output polarity can be swapped. This shouldn't be required for a properly wired device. Finally, the power output to the thermoelectric element is monitored and displayed in units of percent. Typical power outputs are 0–50 %. The power output can be used as a diagnostic for proper functioning of the cooling system. For example, a power output of 100 % at $T=10\,^{\circ}\mathrm{C}$ and combined with a lack of further cooling would indicate that either the heat sink is not working as intended or that the thermoelectric element is damaged and needs replacement.

A brief standard operating procedure is provided below

- 1) Fill in the chilled bath circulator with working liquid (water or ethylene glycol) and switch it on. Set the temperature of coolant below 5 $^{\circ}$ C.
- 2) Turn on N₂ supply at 3 L/min.
- 3) If only a single thermistor is attached, "Read temperature 1" should be the same as the "Set Temperature" when the controller "Power" is in On position. Same temperature readings in Manual mode ensures proper thermistor connection to the cold plate.
- 4) A desired "Experiment Name" (e.g. Test run 1) should be written before starting the experiment.
- 5) Scan range can be selected by setting the "Start" temperature (e.g. $10 \,^{\circ}$ C) and "Stop" temperature (e.g. $-40 \,^{\circ}$ C). For a temperature ramp of $2 \,^{\circ}$ C/min during the experiment, "Duration" will be set as 50 min for "Start" and "Stop" temperatures of $10 \,^{\circ}$ C and $-40 \,^{\circ}$ C.
- 6) Gloves should be worn to prevent contamination of samples. Place the hydrophobic slides on the surface of the cold plate and then place the drops (each of volume $\sim 1~\mu$ L) on the hydrophobic slides. Dimensions of the cold plate allows placing four hydrophobic slides on its surface and it is possible to have around 100 drops on slides during a single experiment.
- 7) To start the experiment, switch from "Manual" to "Ramp". This will start the temperature ramp and capture pictures every two seconds. The pictures are saved with datetime and the name of the experiment (e.g. Test_run_1).
- 8) If it is desired to observe only freezing, temperature control can be switched to "Manual" once all drops on the cold plate have frozen. This will stop the experiment and the data can be processed using steps in section 6.2. If another replicate/new experiment needs to be done, the user can wipe the drops, remove the slides and place new slides for the new run.
- 9) To shut down the system, toggle "Power" switch to Off in the software, turn off the power switch on the back side of the cold stage controller box, turn off nitrogen supply and chilled bath circulator.

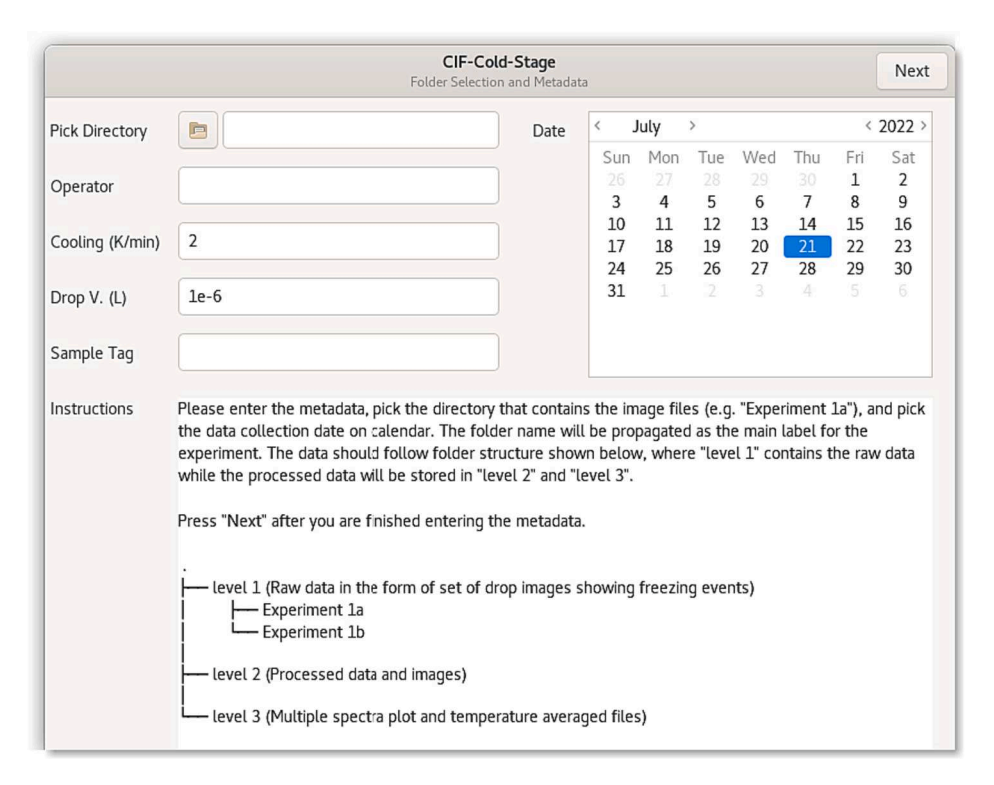


Fig. 7. Image shows the greeter window where metadata needs to be filled for data processing.

Data processing

User guided image analysis software is used to convert images to INP concentration. The core functionality of this software has been described in previous publications [12,24]. Briefly, the software seeks to automatically identify the drops in the image. Canny edge detection followed by a circular Hough transform is used to achieve this. Potentially misclassified drops are corrected by the user. Next the software creates a time lapse for each drop. Freeze events are detected by evaluating change in the average grayscale of the drop. Potentially misclassified drops are corrected by the user. Finally, the quality controlled freeze events are used to compute the fraction of frozen droplets versus temperature, and the concentration of INPs in solution using Vali's formula [18].

Invoking the analysis, software will raise the greeter window shown in Fig. 7. The folder created during the "Ramp" contains all the images of the drop freezing assay experiment and can be opened by clicking "Pick Directory" in the greeter. In addition, fill out the metadata which includes details of operator, cooling rate, drop volume, and sample tag. Use the calendar to set the date of sample collection. Press Next after filling in the metadata. Now the software will parse the image and guess the location of each drop in the image, as shown in Fig. 8. Each red circle corresponds to an identified drop. Some drops are missing a circle, some drops have two or more circles. Drops can be manually chosen by adding/deleting circles as needed. The add/delete function visible on screen can be toggled for adding/deleting circles. Remove all doublets (two in this image). If the user removes any circle by mistake, it can be added again. Removing a circle will effectively ignore the drop in the subsequent processing. The user should ensure one red circle on each drop, which the user wants to process. The panel to the right in Fig. 8 shows the identified edges. Depending on the image contrast, illumination, and droplet size, this edge detection may be insufficient, leading to too many edges and lots of false positive drop detection. The spin button with the value 25 is a hyper parameter that sets the spatial scale in the edge detection algorithm. The user can change the value and press Recalculate Edges to try to improve the center detection. If it performs poorly, you can also press Delete All and then add all drops manually.

Press Next when you are happy with the drop centers. The software will load and tile all images, and transform the data into a stack. It will then search through the stack and identify freeze events. The validation window as shown in Fig. 9 will appear. The freeze detection tries to identify changes in the image that correspond to freezing (indicated by opaque drop). The triplets correspond to an image sequence with suspected freezing. The droplet should turn from clear to opaque either in the second or third image. Sometimes the freeze detection is an error. For example the second and fifth triplet in the left most column of Fig. 9. These can be manually removed as false positives by clicking twice on the triplet. A white line on the second and fifth triplet in the left most column indicates that the drops have been removed and will not be used for final processing. Note that the first click has no effect and the user needs to click twice. If a triplet is accidentally removed, it can be undone by switching the toggle button in the header bar to "Add" and clicking on the triplet once more. Not all drops fit on a single page so the spin button on the top right can be toggled to scan through all the drops. Press Finished once all drops are scanned and false positives are removed by adding white lines. Next the software will create a quick look and write processed data and metadata to the exampledata/level 2/Experiment 1/ folder. Fig. 10 shows a quick look image with INP concentration L⁻¹ water (left) and activated fraction (right) as a function of freezing temperature. The image is written to the level 2 folder. Also written is a comma delimited text file with drop centers and freezing temperatures, a comma delimited text file with the activated fraction and INP concentration vs. temperature, as well as image files that indicate the selected drops, drop centers, accepted drops, and discarded drops. With this the processing of one sample completes and the user can either choose another file directory from the greeter shown in Fig. 7 or can press Close to exit the program.

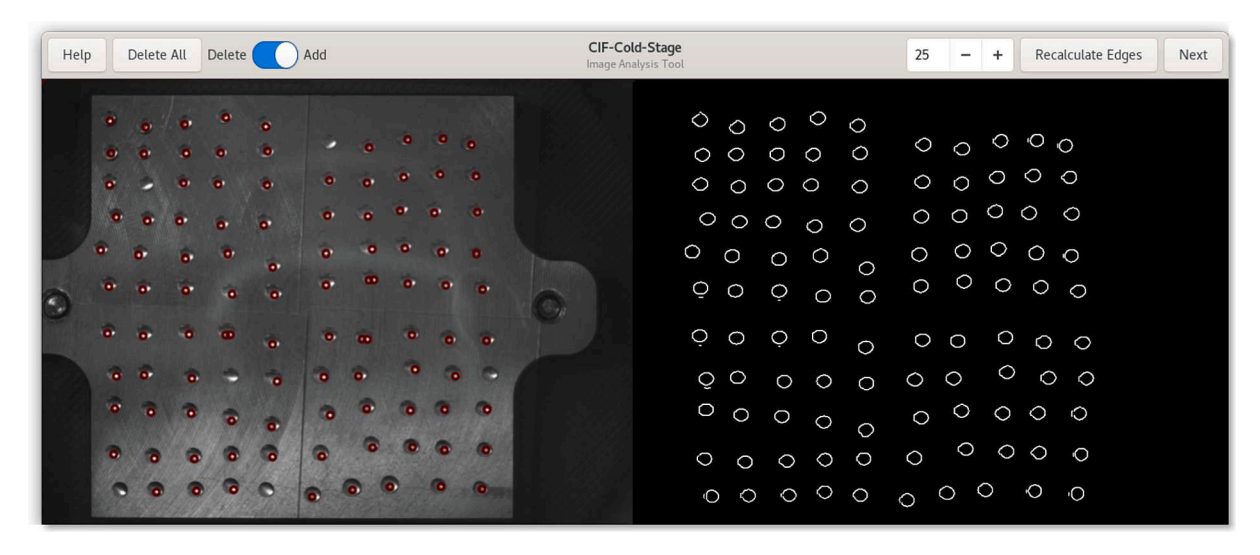


Fig. 8. Left panel of the figure shows the screen where drops are visible on the cold stage and each red circle corresponds to an identified drop, selected for data processing. Right panel shows the identified edges at hyper parameter 25 (in the header bar) that sets the spatial scale in the edge detection algorithm.

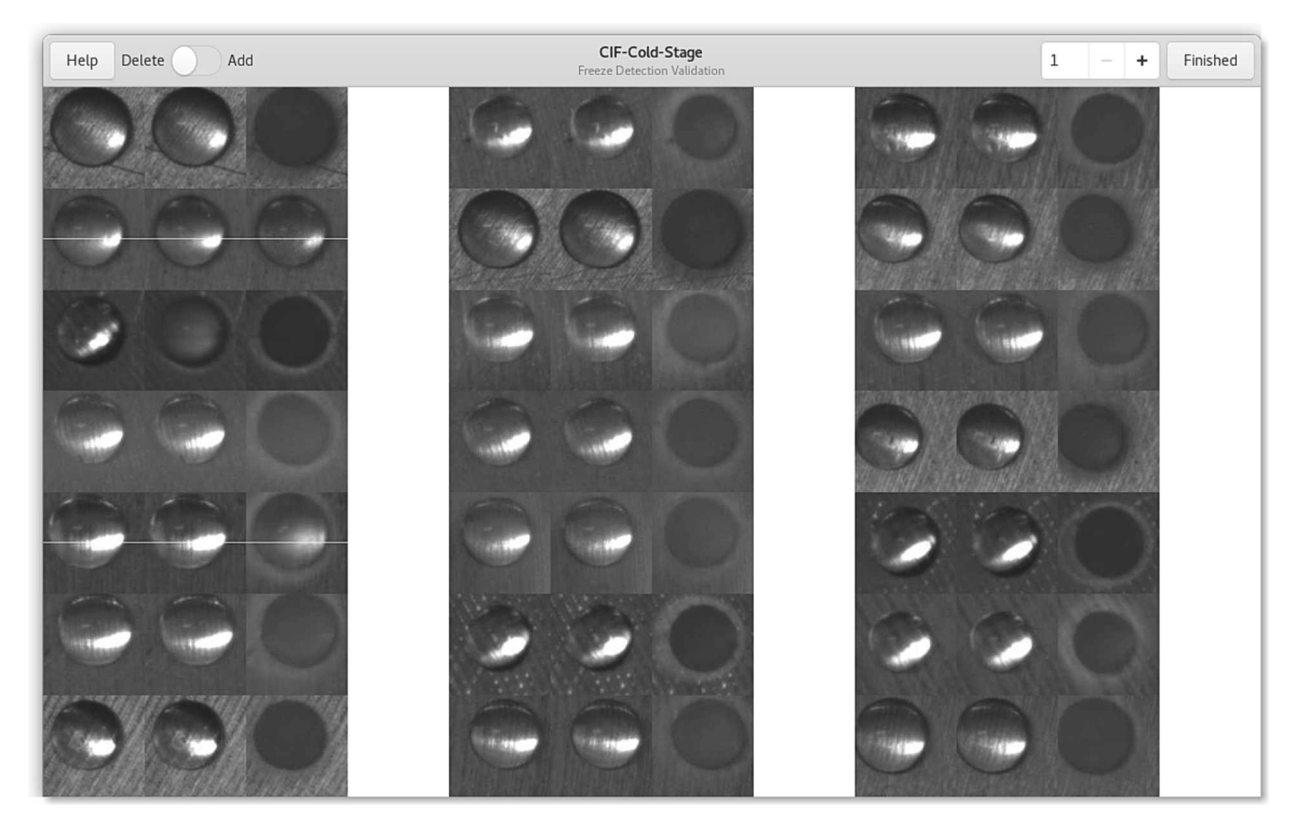


Fig. 9. Validation window showing droplet freezing events for all processed droplets. A white line on the second and fifth triplet in the left most column, which indicates that the drop has been removed and will not be used for final processing.

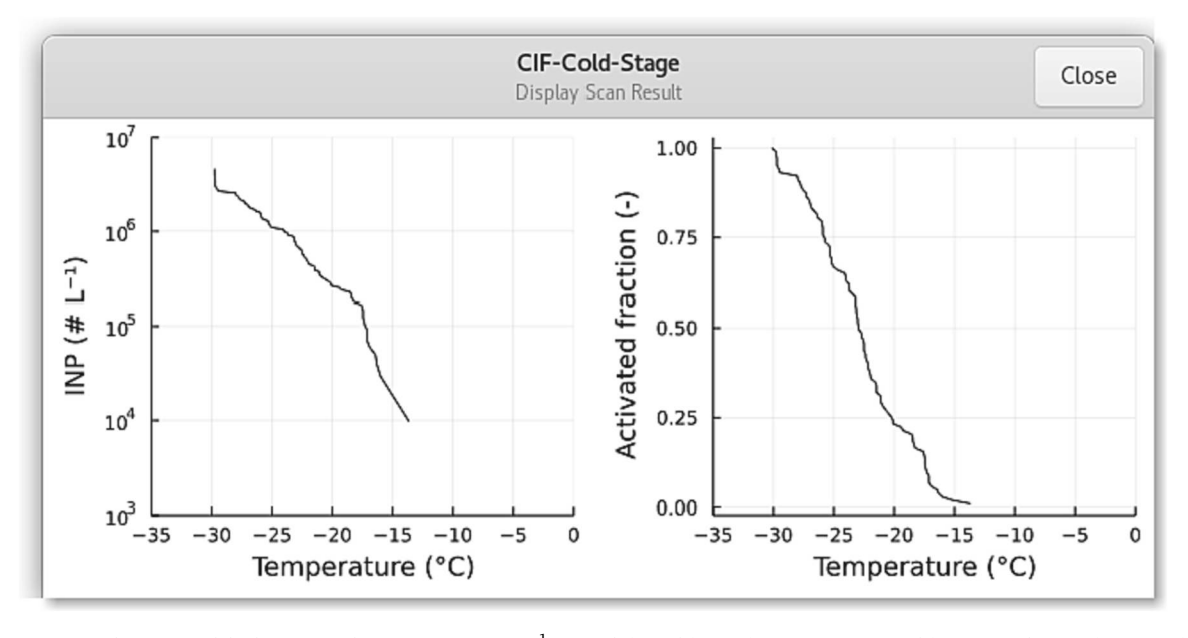


Fig. 10. Figure shows a quick look image with INP concentration L^{-1} water (left) and frozen fraction (or activated fraction, right) as a function of the freezing temperature.

Validation and characterization

The temperature accuracy and spatial heterogeneity of the temperature on the cold stage can be evaluated using "warmup" experiments. In this configuration, the plate is cooled and temperature is allowed to ramp back up to above the melting point of water. Fig. 11 shows the evolution of the image of 21 randomly selected drops from -1 to 4 °C. The change in droplet appearance is gradual, indicating that melting is slower than freezing. At 1 °C all of the drops remain frozen. At 3 °C, all of the drops are melted. The slight warm bias and heterogeneity are due to a combination of effects. First, there is thermal lag between the metal plate and the drops, which is due to the placement of glass slides. Second, the thermistor is embedded in a small hole at the stage. The degree of contact between the tip and the metal depends on how well the thermal paste covers small air gaps in the hole. This may lead to a small difference in metal temperature and the measured temperature. Third, the thermoelectric element may have slight heterogeneity in heat transfer across the surface. Nevertheless, the warmup experiment demonstrates that a conservative estimate of the melting temperature is 2 °C \pm 1 °C. The warm bias is corrected for in subsequent experiments. The magnitude of the warm bias may depend on the cooling rate and seating contact of the thermistor in the aluminum block. It is therefore recommended that users regularly perform this warm up experiment to evaluate the warm bias.

Based on prior work [24], we recommend running experiments in triplicate. A repeat experiment involves placing a new set of glass slides, new drops, and repeating the cooling cycle. A typical performance of a triplicate experiment is shown for ultrapure HPLC grade water (Fisher) in Fig. 12a. Experiments with ultrapure water establish the background against which ice nucleation can be observed for a given substrate [12,31]. We recommend binning the data into 1 °C intervals and compute the average and interquartile range of all drops falling into the interval. A minimum number of drops should be specified per bin. We further recommend setting this value \geq 3. Fig. 12b shows an example of experiments with a suspension of Arizona Test Dust (Powder Technology, Inc.; ISO 12103-1, A4 Coarse) 0.01 % w/w in ultrapure HPLC grade water. Arizona Test Dust (ATD) was used because we have data for this concentration and this particular batch of dust is from prior experiments using the predecessor of the instrument described here [12,31]. Fig. 12b shows that the addition of INPs shifts the freezing curve toward warmer temperatures. The ATD data generated with this version of the cold stage are in good agreement of the INP concentration with those from prior experiments for the same substance.

Summary of performance characteristics

The performance characteristics of the cold stage can be summarized as follows

- · Measurement mode: immersion freezing
- \bullet Cold-stage area: 40 \times 40 mm
- ullet Droplet temperature precision: $\Delta T \pm 1~^{\circ}C$
- Camera resolution: 2592x1944 pixels, full color
- Accessible temperature range: $-40 \, ^{\circ}\text{C} < T < 99 \, ^{\circ}\text{C}$
- Number of drops per experiment: 100 with 1 µL drop volume
- Droplet placement: electronic pipette
- Variable linear cooling rate: ≤ 4 °C/min
- Time per experiment: ≥ 30 min

Note that we tested cooling rates of 4 °C/min and obtained comparable results for Arizona Test Dust (data not shown here). However, at that cooling rate, the temperature heterogeneity and warm bias of the plate increases, and we recommend a cooling rate of 2 °C/min or slower. Reaching the lower temperature limit of -40 °C will require sufficiently cold recirculating cooling liquid (\sim 0 °C).

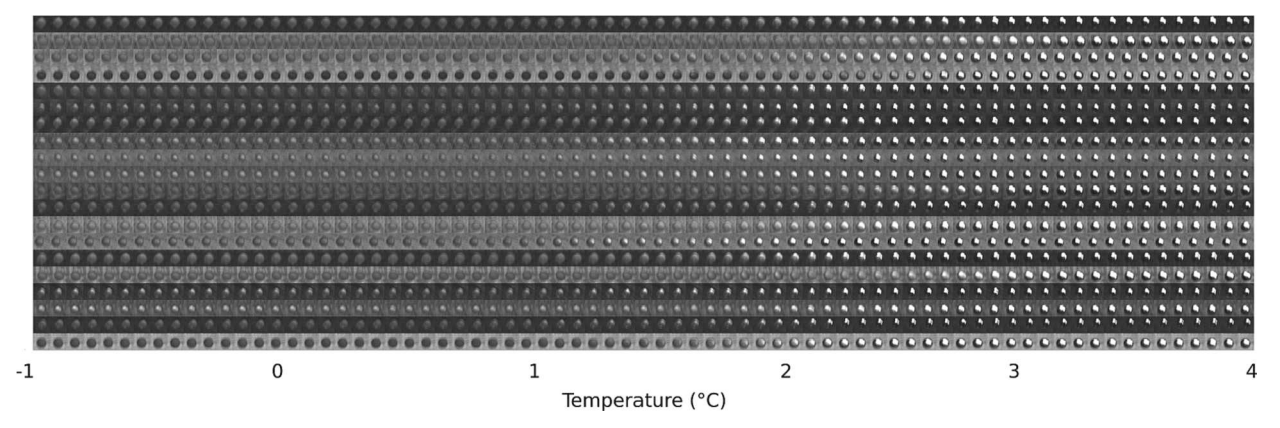


Fig. 11. Example melting mosaic for 21 randomly selected drops and cooling/heating rate of 2 °C min⁻¹.

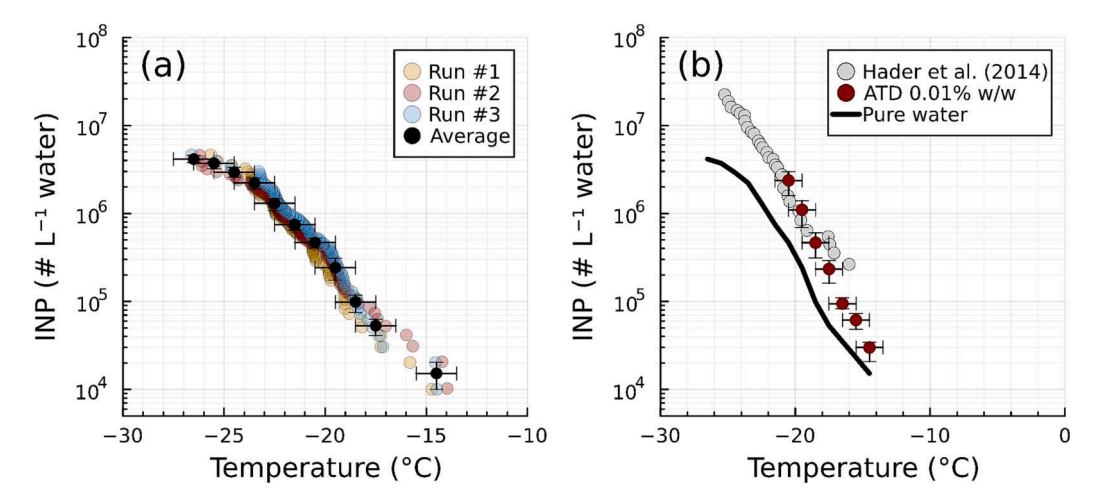


Fig. 12. Ice nucleating particle concentration versus temperature spectra derived from experiments with a cooling rate of $2~^{\circ}$ C min $^{-1}$. (a) Three repeat runs of ultrapure water (colored symbols). The black dots denote the binned average of the three runs. The error bars denote the temperature uncertainty from plate heterogeneity ($\Delta T \pm 1~^{\circ}$ C) and the interquartile range of all observations within the bin. (b) The black line shows the ultrapure water data from panel (a). Red symbols correspond to three repeats of pure Arizona Test Dust suspensions 0.01 % w/w. Gray circles correspond to the nanodrop data from Hader et al. (2014) for Arizona Test Dust suspensions 0.01 % w/w generated from the same dry sample container.

Ethics statements

Not applicable.

CRediT authorship contribution statement

Sunandan Mahant: Investigation, Methodology, Software, Data curation, Writing – original draft. Shweta Yadav: Investigation, Methodology, Software, Writing – original draft. Cameron Gilbert: Investigation. Eva R. Kjærgaard: Investigation. Mads M. Jensen: Methodology. Tommy Kessler: Methodology. Merete Bilde: Writing – review & editing, Supervision, Project administration, Funding acquisition. Markus D. Petters: Conceptualization, Methodology, Software, Formal analysis, Validation, Writing – review & editing, Supervision, Project administration, Funding acquisition.

Declaration of Competing Interest

The authors declare that they have no known competing financial interests or personal relationships that could have appeared to influence the work reported in this paper.

Acknowledgments

This research was supported by the U.S. National Science Foundation grant AGS 2112978. CG acknowledges support from the Office of Undergraduate Research at NC State University. MDP and MB acknowledge support from Aarhus University Research Foundation grant AUFF-E-2021-6-26. MB, ERK, MSJ and TK acknowledge support from Independent Research Fund Denmark (Grant 0217-00442B), SY acknowledges United States-India Educational Foundation (USIEF) for Fulbright Kalam Climate Fellowship award for Postdoctoral Research (Award 2225/FKPDR/2017) and Central University of Jammu for granting study leave.

Appendix A. Supplementary data

Supplementary data to this article can be found online at https://doi.org/10.1016/j.ohx.2023.e00491.

References

^[1] S.M. Kreidenweis, M. Petters, U. Lohmann, 100 Years of Progress in Cloud Physics, Aerosols, and Aerosol Chemistry Research, Meteorol. Monogr. 59 (2019) 11.1–11.72, https://doi.org/10.1175/AMSMONOGRAPHS-D-18-0024.1.

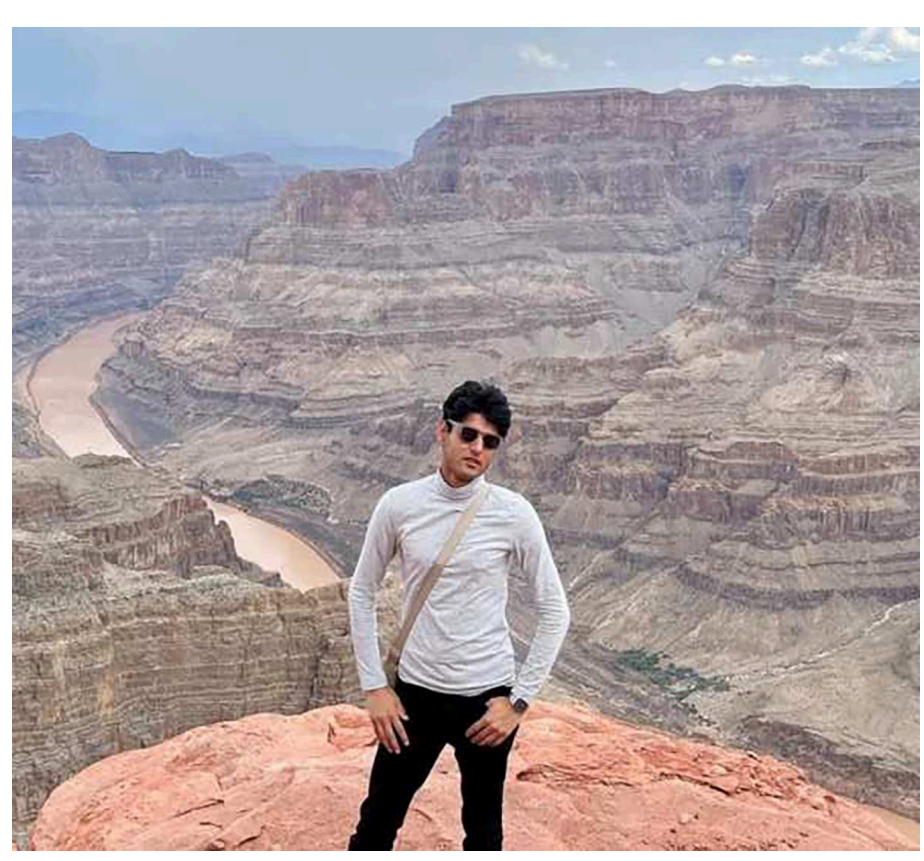
^[2] G. Vali, Nucleation terminology, Bull. Georg. Acad. Sci. Am. Meteorol. Soc. 66 (1985) 1426–1427.

[3] G. Vali, P.J. DeMott, O. Möhler, T.F. Whale, Technical Note: A proposal for ice nucleation terminology, Atmos. Chem. Phys. 15 (2015) 10263–10270, https://doi.org/10.5194/acp-15-10263-2015.

- [4] P.J. DeMott, O. Möhler, O. Stetzer, G. Vali, Z. Levin, M.D. Petters, et al., Resurgence in Ice Nuclei Measurement Research, Bull. Am. Meteorol. Soc. 92 (2011) 1623–1635. https://doi.org/10.1175/2011BAMS3119.1.
- [5] O. Möhler, M. Adams, L. Lacher, F. Vogel, J. Nadolny, R. Ullrich, et al., The portable ice nucleation experiment PINE: a new online instrument for laboratory studies and automated long-term field observations of ice-nucleating particles, Atmos. Meas. Tech. Discuss. 2020 (2020) 1–43, https://doi.org/10.5194/amt-2020-307
- [6] R. Wagner, K. Höhler, W. Huang, A. Kiselev, O. Möhler, C. Mohr, et al., Heterogeneous ice nucleation of α-pinene SOA particles before and after ice cloud processing, J. Geophys. Res. Atmos. 122 (2017) 4924–4943, https://doi.org/10.1002/2016JD026401.
- [7] D.C. Rogers, P.J. DeMott, S.M. Kreidenweis, Y. Chen, A Continuous-Flow Diffusion Chamber for Airborne Measurements of Ice Nuclei, J. Atmos. Ocean Technol. 18 (2001) 725–741, https://doi.org/10.1175/1520-0426(2001)018
- [8] Petters MD, Parsons MT, Prenni AJ, DeMott PJ, Kreidenweis SM, Carrico CM, et al. Ice nuclei emissions from biomass burning. J Geophys Res Atmospheres 2009;114. https://doi.org/doi:10.1029/2008JD011532.
- [9] S. Garimella, T.B. Kristensen, K. Ignatius, A. Welti, J. Voigtländer, G.R. Kulkarni, et al., The SPectrometer for Ice Nuclei (SPIN): an instrument to investigate ice nucleation, Atmos. Meas. Tech. 9 (2016) 2781–2795, https://doi.org/10.5194/amt-9-2781-2016.
- [10] G. Kulkarni, N. Hiranuma, O. Möhler, K. Höhler, S. China, D.J. Cziczo, et al., A new method for operating a continuous flow diffusion chamber to investigate immersion freezing: assessment and performance study, Atmos. Meas. Tech. Discuss. 2020 (2020) 1–27, https://doi.org/10.5194/amt-2019-386.
- [11] P.J. DeMott, O. Möhler, D.J. Cziczo, N. Hiranuma, M.D. Petters, S.S. Petters, et al., The Fifth International Workshop on Ice Nucleation phase 2 (FIN-02): Laboratory intercomparison of ice nucleation measurements, Atmos. Meas. Tech. Discuss. 2018 (2018) 1–44, https://doi.org/10.5194/amt-2018-191.
- [12] T.P. Wright, M.D. Petters, The role of time in heterogeneous freezing nucleation, J. Geophys. Res. Atmos. 118 (2013) 3731–3743, https://doi.org/10.1002/jerd.50365.
- [13] M. Polen, E. Lawlis, R.C. Sullivan, The unstable ice nucleation properties of Snomax® bacterial particles, J. Geophys. Res. Atmos. 121 (11) (2016) 666–678, https://doi.org/10.1002/2016JD025251.
- [14] E.K. Bigg, A new Technique for Counting Ice-Forming Nuclei in Aerosols, Tellus 9 (1957) 394-400, https://doi.org/10.1111/j.2153-3490.1957.tb01895.x.
- [15] C. Budke, T. Koop, BINARY: an optical freezing array for assessing temperature and time dependence of heterogeneous ice nucleation, Atmos. Meas. Tech. 8 (2015) 689–703, https://doi.org/10.5194/amt-8-689-2015.
- [16] T.F. Whale, B.J. Murray, D. O'Sullivan, T.W. Wilson, N.S. Umo, K.J. Baustian, et al., A technique for quantifying heterogeneous ice nucleation in microlitre supercooled water droplets, Atmos. Meas. Tech. 8 (2015) 2437–2447, https://doi.org/10.5194/amt-8-2437-2015.
- [17] M.D. Tarn, S.N.F. Sikora, G.C.E. Porter, B.V. Wyld, M. Alayof, N. Reicher, et al., On-chip analysis of atmospheric ice-nucleating particles in continuous flow, Lab Chip 20 (2020) 2889–2910, https://doi.org/10.1039/DOLC00251H.
- [18] G. Vali, Quantitative Evaluation of Experimental Results and the Heterogeneous Freezing Nucleation of Supercooled Liquids, J. Atmos. Sci 28 (1971) 402–409, https://doi.org/10.1175/1520-0469(1971)028<0402;QEOERA>2.0.CO;2.
- [19] M.J. Wheeler, A.K. Bertram, Deposition nucleation on mineral dust particles: a case against classical nucleation theory with the assumption of a single contact angle, Atmos. Chem. Phys. 12 (2012) 1189–1201, https://doi.org/10.5194/acp-12-1189-2012.
- [20] B. Wang, A.T. Lambe, P. Massoli, T.B. Onasch, P. Davidovits, D.R. Worsnop, et al., The deposition ice nucleation and immersion freezing potential of amorphous secondary organic aerosol: Pathways for ice and mixed-phase cloud formation, J. Geophys. Res. Atmos. 117 (2012), https://doi.org/10.1029/2012JD018063.
- [21] J.C. Charnawskas, P.A. Alpert, A.T. Lambe, T. Berkemeier, R.E. O'Brien, P. Massoli, et al., Condensed-phase biogenic–anthropogenic interactions with implications for cold cloud formation, Faraday Discuss. 200 (2017) 165–194, https://doi.org/10.1039/C7FD00010C.
- [22] J. Schrod, A. Danielczok, D. Weber, M. Ebert, E.S. Thomson, H.G. Bingemer, Re-evaluating the Frankfurt isothermal static diffusion chamber for ice nucleation, Atmos. Meas. Tech. 9 (2016) 1313–1324, https://doi.org/10.5194/amt-9-1313-2016.
- [23] M.D. Petters, T.P. Wright, Revisiting ice nucleation from precipitation samples, Geophys. Res. Lett. 42 (2015) 8758–8766, https://doi.org/10.1002/ 2015GL065733
- [24] S. Yadav, R.E. Venezia, R.W. Paerl, M.D. Petters, Characterization of Ice-Nucleating Particles Over Northern India, J. Geophys. Res. Atmos. 124 (2019) 10467–10482, https://doi.org/10.1029/2019JD030702.
- [25] Yadav S, Curtis NP, Venezia RE, Tandon A, Paerl RW, Petters MD. Bioaerosol Diversity and Ice Nucleating Particles in the North-Western Himalayan Region. J Geophys Res Atmospheres 2022;127:e2021JD036299. https://doi.org/10.1029/2021JD036299.
- [26] A.J. Durant, R.A. Shaw, Evaporation freezing by contact nucleation inside-out, Geophys. Res. Lett. 32 (2005), https://doi.org/10.1029/2005GL024175.
- [27] A.P. Fornea, S.D. Brooks, J.B. Dooley, A. Saha, Heterogeneous freezing of ice on atmospheric aerosols containing ash, soot, and soil, J. Geophys. Res. Atmos. 114 (2009), https://doi.org/10.1029/2009JD011958.
- [28] C.W. Gurganus, J.C. Charnawskas, A.B. Kostinski, R.A. Shaw, Nucleation at the Contact Line Observed on Nanotextured Surfaces, Phys. Rev. Lett. 113 (2014), 235701, https://doi.org/10.1103/PhysRevLett.113.235701.
- [29] F. Yang, R.A. Shaw, C.W. Gurganus, S.K. Chong, Y.K. Yap, Ice nucleation at the contact line triggered by transient electrowetting fields, Appl. Phys. Lett. 107 (2015), 264101, https://doi.org/10.1063/1.4938749.
- [30] P.J. DeMott, T.C., Hill, M.D. Petters, A.K. Bertram, Y. Tobo, R.H. Mason, et al., Comparative measurements of ambient atmospheric concentrations of ice nucleating particles using multiple immersion freezing methods and a continuous flow diffusion chamber, Atmos. Chem. Phys. 17 (2017) 11227–11245, https://doi.org/10.5194/acp-17-11227-2017.
- [31] J.D. Hader, T.P. Wright, M.D. Petters, Contribution of pollen to atmospheric ice nuclei concentrations, Atmos. Chem. Phys. 14 (2014) 5433–5449, https://doi.org/10.5194/acp-14-5433-2014.
- [32] T.P. Wright, J.D. Hader, G.R. McMeeking, M.D. Petters, High Relative Humidity as a Trigger for Widespread Release of Ice Nuclei, Aerosol. Sci. Technol. 48 (2014) i-v, https://doi.org/10.1080/02786826.2014.968244.
- [33] J. Chen, Z. Wu, S. Augustin-Bauditz, S. Grawe, M. Hartmann, X. Pei, et al., Ice-nucleating particle concentrations unaffected by urban air pollution in Beijing, China, Atmos. Chem. Phys. 18 (2018) 3523–3539, https://doi.org/10.5194/acp-18-3523-2018.
- [34] A. Welti, E.K. Bigg, P.J. DeMott, X. Gong, M. Hartmann, M. Harvey, et al., Ship-based measurements of ice nuclei concentrations over the Arctic, Atlantic, Pacific and Southern Ocean, Atmos. Chem. Phys. Discuss. 2020 (2020) 1–22, https://doi.org/10.5194/acp-2020-466.
- [35] C.S. McCluskey, T.C.J. Hill, R.S. Humphries, A.M. Rauker, S. Moreau, P.G. Strutton, et al., Observations of Ice Nucleating Particles Over Southern Ocean Waters, Geophys. Res. Lett. 45 (11) (2018), https://doi.org/10.1029/2018GL079981.
- [36] C. Jimenez-Sanchez, R. Hanlon, K.A. Aho, C. Powers, C.E. Morris, D.G. Schmale, Diversity and ice nucleation activity of microorganisms collected with a small unmanned aircraft system (sUAS) in france and the united states, Front. Microbiol. 9 (2018) 1667, https://doi.org/10.3389/fmicb.2018.01667.
- [37] G.C.E. Porter, S.N.F. Sikora, M.P. Adams, U. Proske, A.D. Harrison, M.D. Tarn, et al., Resolving the size of ice-nucleating particles with a balloon deployable aerosol sampler: the SHARK, Atmos. Meas. Tech. 13 (2020) 2905–2921, https://doi.org/10.5194/amt-13-2905-2020.
- [38] H.C. Price, K.J. Baustian, J.B. McQuaid, A. Blyth, K.N. Bower, T. Choularton, et al., Atmospheric Ice-Nucleating Particles in the Dusty Tropical Atlantic, J. Geophys. Res. Atmos. 123 (2018) 2175–2193, https://doi.org/10.1002/2017JD027560.
- [39] H. Kiani, D.-W. Sun, Water crystallization and its importance to freezing of foods: A review, Trends Food Sci. Technol. 22 (2011) 407–426, https://doi.org/10.1016/j.tifs.2011.04.011.
- [40] G.J. Morris, E. Acton, Controlled ice nucleation in cryopreservation-a review, Cryobiology 66 (2013) 85-92, https://doi.org/10.1016/j.cryobiol.2012.11.007.
- [41] R. Geidobler, G. Winter, Controlled ice nucleation in the field of freeze-drying: fundamentals and technology review, Eur J Pharm Biopharm off J Arbeitsgemeinschaft Pharm Verfahrenstechnik EV 85 (2013) 214–222, https://doi.org/10.1016/j.ejpb.2013.04.014.
- [42] T.P. Wright, M.D. Petters, J.D. Hader, T. Morton, A.L. Holder, Minimal cooling rate dependence of ice nuclei activity in the immersion mode, J Geophys Res Atmospheres 118 (10) (2013), https://doi.org/10.1002/jgrd.50810.

[43] G.C. Cornwell, C.M. Sultana, M.D. Petters, H. Al-Mashat, N.E. Rothfuss, O. Möhler, et al., Discrimination between individual dust and bioparticles using aerosol time-of-flight mass spectrometry, Aerosol Sci Technol 56 (2022) 592–608, https://doi.org/10.1080/02786826.2022.2055994.

- [44] N. Hiranuma, S. Augustin-Bauditz, H. Bingemer, C. Budke, J. Curtius, A. Danielczok, et al., A comprehensive laboratory study on the immersion freezing behavior of illite NX particles: a comparison of 17 ice nucleation measurement techniques, Atmospheric Chem Phys 15 (2015) 2489–2518, https://doi.org/ 10.5194/acp-15-2489-2015.
- [45] N. Hiranuma, K. Adachi, D.M. Bell, F. Belosi, H. Beydoun, B. Bhaduri, et al., A comprehensive characterization of ice nucleation by three different types of cellulose particles immersed in water, Atmospheric Chem Phys 19 (2019) 4823–4849, https://doi.org/10.5194/acp-19-4823-2019.
- [46] J. Bezanson, A. Edelman, S. Karpinski, V.B. Shah, Julia: A Fresh Approach to Numerical Computing, SIAM Rev. 59 (2017) 65–98, https://doi.org/10.1137/ 141000671.



Sunandan Mahant was a Ph.D. student in the Department of Marine, Earth, and Atmospheric Sciences, North Carolina State University 2021-2023 and is continuing his PhD at the Department of Chemical and Environmental Engineering at the University of California, Riverside. He completed B.S. (Chemistry) degree in 2017 and M.S. (Environmental Sciences) degree in 2020. His research interest is investigating properties of atmospheric aerosols, and understanding climatic impact. His graduate work focuses on characterizing the influence of diameter on particle viscosity.